

Heat and momentum transport in turbulent horizontal convection at low Prandtl numbers

Pierre-Yves Passaggia*

Alberto Scotti†

Brian L. White‡

August 2, 2021

Abstract

The transition to a new turbulent regime in horizontal convection in the case of low Prandtl numbers is analyzed using the Shishkina, Grossmann & Lohse (SGL) theory. The flow driven by the horizontal gradient along a horizontal surface, perpendicular to the acceleration of gravity is shown to transition to turbulence in the plume and the core. This transition to turbulence sets a sequence of heat transfer and momentum transport scalings which are found to follow the SGL prediction for the scaling factors and the prediction of Hughes, Griffith & Mullarney (HGM) for larger forcing amplitudes. These results embed the HGM model in the SGL theory, agreed and extends the known regime diagram of horizontal convection, and provide the first evidence of both regimes at low and intermediate Prandtl numbers and sheds new insights on the role of HC in the earth's inner core dynamics.

Turbulent Horizontal Convection (HC) in highly thermally conductive liquids plays a major role in geophysical flows. For example, it drives the Earth's outer core dynamics via either heat transport from the inner to the outer core [2] or Joule effect due to Earth's magnetic field [20]. Although a lot of attention has been devoted to Rayleigh-Bénard Convection (RBC) for the outer core's dynamics, it is only very recently that HC has attracted the attention of planetary scientists [1]. Lateral motions in the outer core are responsible for driving large scale horizontal flows in the mantle and have long been thought to be at the origin of striping and faulting of tectonic plates and strike-slip earthquakes [7]. At the edge of Earth's inner core, horizontal regions of thermally stable (crystallizing) and unstable (melting) stratified layers explain the East-West asymmetry of the inner core [1]. However, only very little is known about the properties of the turbulent horizontal flows generated in these regions. In this letter, we report Direct Numerical Simulation (DNS) results on how the Reynolds number (Re), the turbulent kinetic energy dissipation (ϵ_u) and the Nusselt number (Nu) depend on the Rayleigh number (Ra) and the Prandtl number (Pr) in turbulent HC at low Pr for different Prandtl numbers characteristic of convection in gases where $0.1 < \text{Pr} < 1$ [11, 21], and liquid metals where $\text{Pr} = \mathcal{O}(10^{-2})$ (see ref.[20]). The results are in agreement with the scaling power laws recently derived by Shishkina *et al.* [16] based on the original work of Grossmann & Lohse [4] (GL) and numerical simulations of Takehiro [20]. It also provides a connection between the GL theory and the plume driven dynamics derived by Hughes *et al.* [6]. Our simulations cover the laminar Rossby regime I_l (see ref.[12]), the high-Pr laminar regime I_l^* recently reported by Shishkina & Wagner [17] and a new low-Pr turbulent regimes named II_l (see ref.[19, 4] for theoretical predictions of HC and RBC), which is the first turbulent limiting regime reported in HC. We also observe the plume dominated flow regime of Hughes *et al.*

*Department of Marine Sciences, University of North Carolina, Chapel Hill, NC 27599, USA. Email: passaggia@unc.edu.

†Department of Marine Sciences, University of North Carolina, Chapel Hill, NC 27599, USA. Email: ascotti@unc.edu.

‡Department of Marine Sciences, University of North Carolina, Chapel Hill, NC 27599, USA. Email: bwhite@unc.edu.

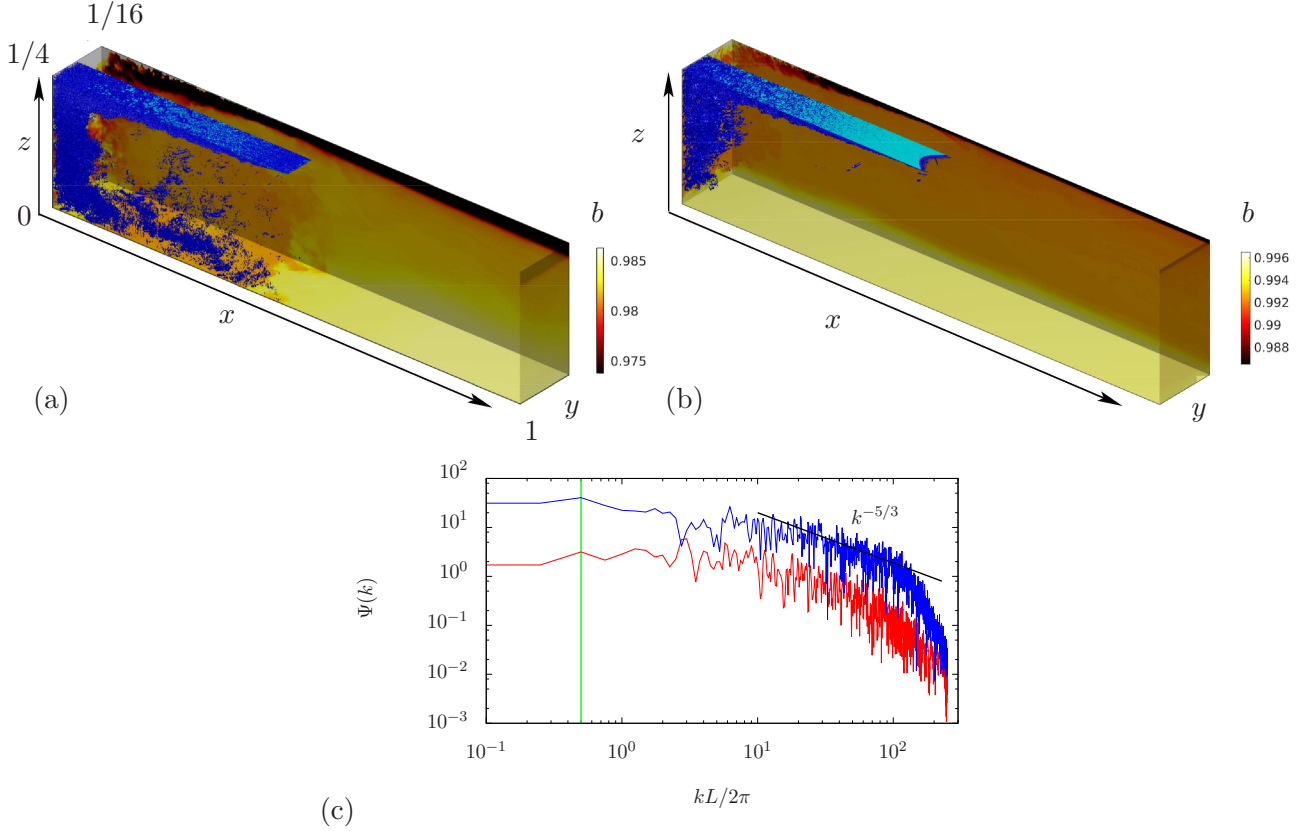


Figure 1: Snapshot of the iso-contours of $\Lambda_2 = -Pr^{-1}/8$ criteria (blue) and buoyancy b (background) at (a) $Ra = 6.4 \times 10^{13}$, $Pr = 0.01$ showing the new regime (II_l) and (b) $Ra = 6.4 \times 10^{13}$, $Pr = 1$ corresponding to the Hughes' regime [6] (II_u). (c) Turbulent spectra $\Psi(k)$ at $Ra = 6.4 \times 10^{13}$ at $Pr = 0.05$ (red) and $\Psi(k)/2$ at $Pr = 1$ (blue) for the same Ra . The black line shows the $k^{-5/3}$ turbulence cascade whereas the green vertical line shows the wavenumber of the forcing.

(see ref.[6]), that we name II_u according to the SGL theory. These results also agree and extend the regime diagram of horizontal convection proposed in Hughes & Griffith (see ref.[5]).

Similarly to Shishkina & Wagner [17], we exploit the idea that in turbulent thermal convection, the time- and volume-averaged thermal and viscous dissipation rates are determined to leading order by their bulk or Boundary Layer (BL) contributions. For the ease of comparison, we follow the same way of presenting as Shishkina & Wagner [17]. We consider here the problem of convection in the Boussinesq limit, where the density difference $\Delta\rho = \rho_{max} - \rho_{min}$ across the horizontal surface is a small deviation from the reference density ρ_{min} . In this limit, the equations of fluid motion are

$$\frac{D\mathbf{u}}{Dt} = -\nabla p + b\mathbf{e}_z + \left(\frac{Pr}{Ra}\right)^{1/2} \nabla^2 \mathbf{u} \quad (1a)$$

$$\nabla \cdot \mathbf{u} = 0 \quad (1b)$$

$$\frac{Db}{Dt} = (Pr Ra)^{-1/2} \nabla^2 b, \quad (1c)$$

where D/Dt denotes the material derivative, $\mathbf{u} = (u, v, w)^T$ is the velocity vector, $b = -g(\rho - \rho_{min})/\rho_{min}$ is the buoyancy, g is the acceleration of gravity along the vertical unit vector \mathbf{e}_z and p is the hydrodynamic pressure. The Prandtl number is given by $Pr = \nu/\kappa$ where ν and κ are

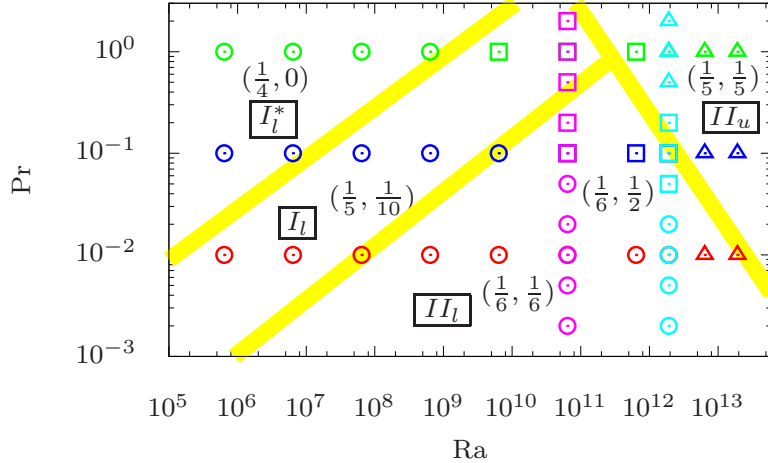


Figure 2: (a) Sketch of the phase diagram in the (Ra, Pr) plane for the laminar regimes I_l and I_l^* together with the turbulent scalings II_l with the conducted DNS. The yellow stripes shows the transition from I_l^* to I_l , and I_l to II_l , with a slope $Pr \approx Ra^{1/2}$. The transition from II_l to II_u with a slope $Pr \approx Ra^{-1}$. Symbols reflect the computational meshes in (x, y, z) , used in the DNS: $512 \times 256 \times 256$ (circle), $1024 \times 384 \times 128$ (squares), and $2048 \times 256 \times 256$ (squares). The values (α, β) in each region provide the exponents $Nu \sim Ra^\alpha Pr^\beta$ measured in the DNS and derived in the theory.

the viscous and stratifying agent's diffusion coefficients. The Navier-Stokes equations are solved on a Cartesian grid, stretched near the upper boundary using second-order finite volumes while the pressure is solved using a standard projection method. Laminar and turbulent flow solutions were integrated in time using an explicit second order Adams-Bashforth type-scheme. The Rayleigh number is defined such that $Ra = \Delta L^3 / (\nu \kappa)$ where L is the horizontal length scale of the domain and $\Delta = -g(\rho_{max} - \rho_{min}) / \rho_{min}$. The computational domain is a parallelepiped of aspect ratio $\Gamma = 4$ with dimensions $[L, W, H] = [1, 1/8, 1/4]$ where W is the width of the computational domain [13]. A buoyancy profile is imposed at the surface $z = H$ where H is the height of the domain using a buoyancy profile such that $b(x)|_{z=H} = (1 + \tanh(9.5x)) / 2$ (see ref.[10]). Since we are interested in turbulence dominated regimes where the scaling is not determined by the buoyancy forcing profile, nor the aspect ratio [16, 15], nor the type of boundary condition, free-slip boundary conditions are used for the velocity on the upper, lower and end walls at $x = \pm L/2$ (see ref.[14]) while the domain is assumed periodic in the transverse direction y . This is in contrast with Shishkina & Wagner[17] where they used no-slip boundary conditions and end walls in the transverse direction. Our approach avoids the numerical difficulties involved with resolving the no-slip BL and a finite domain in the transverse direction. Instead we privilege numerical efficiency and report results for Ra up to 6.4×10^{13} for a wide range of Prandtl numbers.

The turbulent scalings for momentum and buoyancy transport are computed using Direct Numerical Simulations (DNS) in the range $Ra = [6.4 \times 10^5, 6.4 \times 10^{13}]$ and $0.002 \leq Pr \leq 2$. For $Ra < 10^8$ and $0.5 \leq Pr \leq 2$, the HC flows are steady [17, 10]. With increasing Ra and/or decreasing values of Pr , HC flows become increasingly unsteady, leading to turbulence (as shown in figure 1(c)) and the mesh size is increased in order to resolve the Kolmogorov length scale (see ref.[14] for details about turbulent HC). Mesh sizes are reported in Fig.2(b) in the (Ra, Pr) plane along with the different regimes reported later in this manuscript. Note that turbulence in HC for moderate values of Pr is confined to a narrow region located under the cooling/heavy boundary consisting of the plume and the BL where the fluid is statically unstable (cf. Fig.1) [3, 14]. Decreasing values of Pr

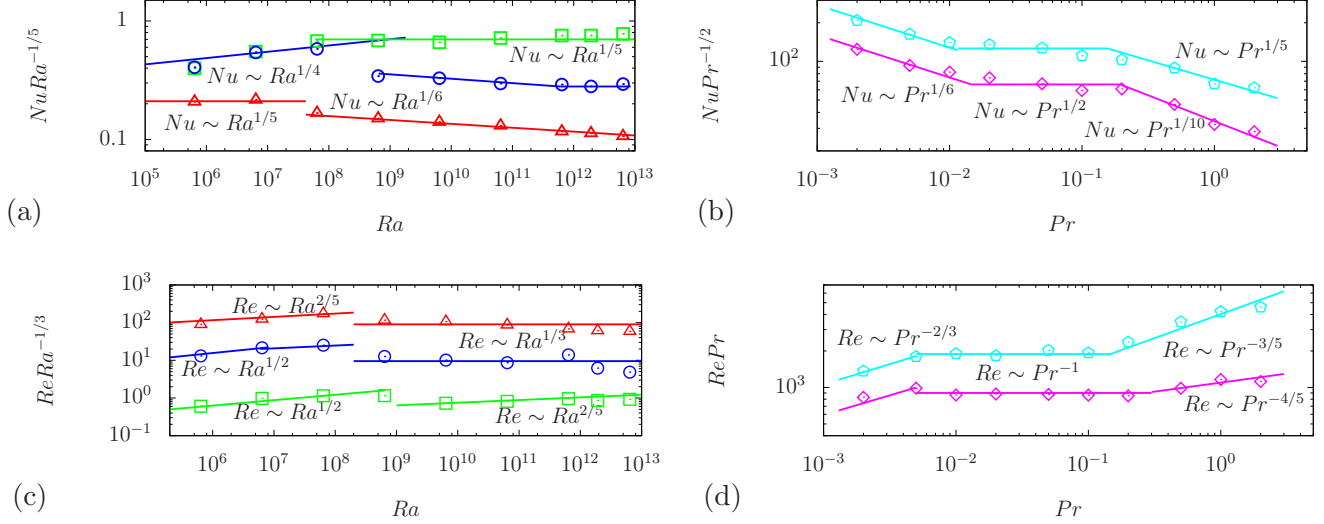


Figure 3: (a),(c) Ra dependencies and (b),(d) Pr dependencies of (a),(b) the Nusselt number and (c),(d) the Reynolds number, as obtained in the DNS for (a),(c) $Pr = 1$ (squares), $Pr = 0.1$ (circles), $Pr = 0.01$ (triangles) and for (b),(d) $Ra = 6.4 \times 10^{10}$ (diamonds) and $Ra = 1.92 \times 10^{12}$ (pentagones). Pr dependence of $\bar{\epsilon}_u$ with Re (d). The DNS results support the scaling in the regime I_l (solid lines) [Eqs. (7a) and (7b)], transition to II_l (dotted lines) [Eqs. (9a),(9b) and (11),(11)], transition to II_u (dotted lines) [Eqs. (14a) and (14b)].

increases the volume of fluid subject to turbulence (see Fig.1) and extends the depth of the circulation.

The dependences of Nu and Re with respect to Ra and Pr are summarized in Fig. 3(a-d). For all values of Pr and Ra, the Nusselt number $Nu \sim Ra^\alpha$ [see Fig. 3(a)] transitions from:

- the enhanced laminar scaling $\alpha = 1/4$ for low Ra,
- the classical laminar scaling $\alpha = 1/5$ for higher Ra,
- A new $\alpha = 1/6$ exponent for small Pr, and
- the entrainment-type regime $\alpha = 1/5$ at even higher Ra.

The magnitude of the large-scale flow is given by $Re = (\overline{\mathbf{u} \cdot \mathbf{u}})^{1/2} L / \nu$ where the overbar denotes the spatio-temporal average over the computational domain. We observe the laminar scalings $Re \sim Ra^\gamma$ with $\gamma = 1/2$ (see ref. [17]) and $\gamma = 2/5$ (see ref.[12]). At higher Ra, the new scaling $\gamma = 1/3$ is also observed and changes back to $\gamma = 2/5$ (see ref.[6]) [Fig. 3(c)]. The low Pr values show a dependence on $Nu \sim Pr^\beta$ with:

- $\beta = 1/2$ for higher Pr and low Ra (see ref. [17]),
- $\beta = 1/10$ for $Ra < 10^{11}$ see (see ref.[12]),
- the new exponent $\beta = 1/6$ at low Pr, and
- $\beta = 1/5$ for $Ra > 5 \times 10^{11}$ see (see ref.[6]).

The Reynolds number dependence $Re \sim Pr^\delta$ with $\delta = -2/3$ for the smaller value of Pr, then $\delta = -1$ for $10^{-2} \lesssim Pr \lesssim 0.2$ changes to $\delta = -4/5$ for increasing Ra at all Pr and increases at high Ra to the

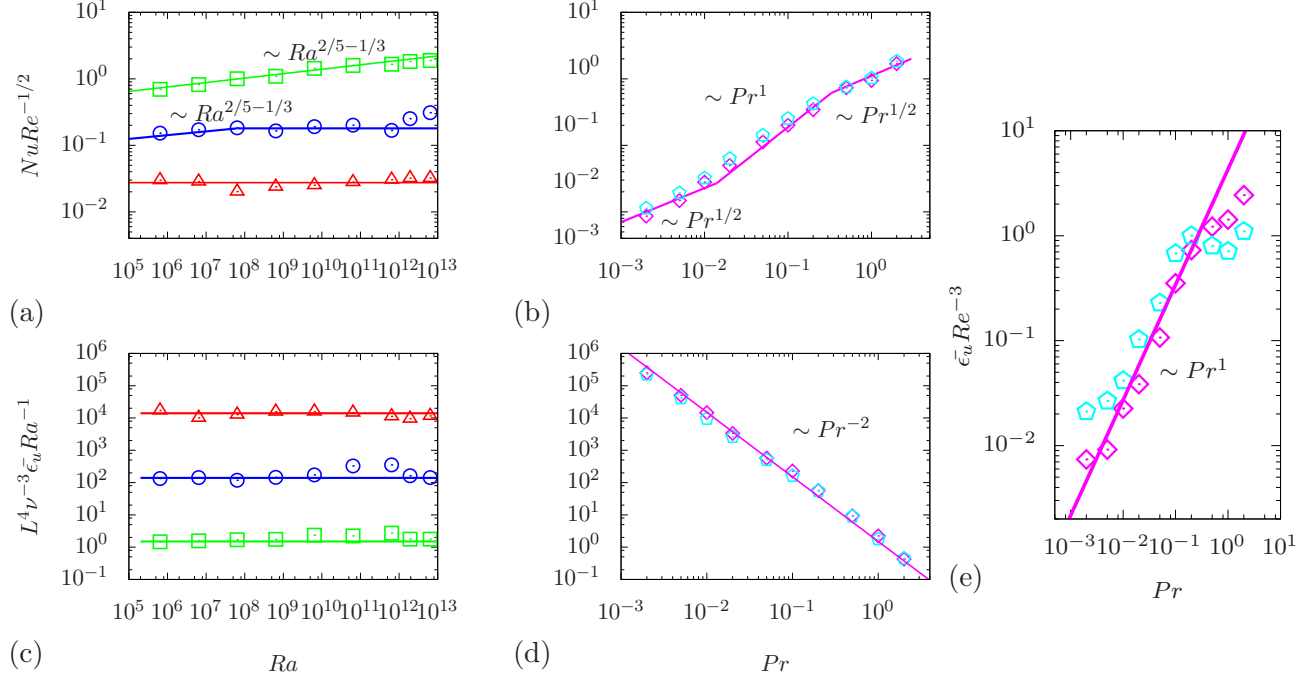


Figure 4: (a),(c) Ra dependences and (b),(d) Pr dependences of (a),(b) $NuRe^{-1/2}$ and (c),(d) $L^4\nu^{-3}\bar{\epsilon}_u Ra^{-1}$, as obtained in the DNS for (a),(c) $Pr = 1$ (squares), $Pr = 0.1$ (circles), $Pr = 0.01$ (triangles) and for (b),(d) $Ra = 10^9$ (diamonds) and $Ra = 2 \times 10^{10}$ (pentagones). The upper figures support (3) and (11b), while the lower figures illustrate (6). The correction in (e) supports the scaling (10).

HGM scaling $\delta = -3/5$ for the larger values of Ra [Fig.3(d)].

The scalings obtained from the DNS can be derived from eq. (1c) for the steady thermal BL equation which writes [4, 18]

$$ub_x + vb_z = \kappa b_{zz}, \quad (2)$$

and reduces to $U\Delta/L = \kappa\Delta/\lambda_b^2$ where λ_b is the thickness of the thermal BL, which scales as $\lambda_b \sim Nu^{-1}$. Combining the above reduces to

$$Nu = Re^{1/2}Pr^{1/2}, \quad (3)$$

and provides a relation tying Nu , Re and Pr . This result is supported by our DNS of laminar to turbulent HC [Fig. 4(a)], for small Pr . A small correction was found for $Pr = 1$ and can also be observed in the laminar DNS described in ref.[17]. Also note that the Prandtl number dependence on (3) is modified from $\sim Pr^{1/2}$ to $\sim Pr^1$ for $10^{-2} \lesssim Pr \lesssim 0.2$ and is associated with the modification of the flow [see Fig. 1(a,b)] which will be explained later.

Paparella and Young (PY) [9] showed that the amount of kinetic energy dissipation in HC is bounded. The time and volume average of eq. (1c) in combination with eq. (1b) give $\langle \partial b / \partial z \rangle_{z=H} = 0$ where $\langle \rangle_{z=H}$ denotes the surface and time average at $z = H$. Combining the time average of eq. (1c) with the PY constraint (i.e. $\langle wb \rangle_z = \kappa \langle \partial b / \partial z \rangle_z$) (see ref.[9]), and integrating over z leads to

$$\overline{wb} \leq \kappa (\langle b \rangle_{z=H} - \langle b \rangle_{z=0}) / H = B(\Gamma/2)\kappa\Delta/L, \quad (4)$$

where $1 < B < 0$ is an arbitrary constant [17]. Taking the kinetic energy equation, time and volume

averaging,

$$\overline{\epsilon_u} = \overline{wb} \leq B(\Gamma/2)\nu^3 L^{-4} \text{RaPr}^{-2}, \quad (5)$$

which is supported for all regimes. SGL recast this argument in a spatio-temporal volume-averaged kinetic energy dissipation rate $\overline{\epsilon_u} \equiv \nu \sum_{i,j} (\partial u_j / \partial x_i)^2$ which in the case of a BL-dominated regime, matches the dissipation in the boundary layer $\overline{\epsilon_u} \sim (\nu U^2) / (\lambda_u L)$ where λ_u is the thickness of the viscous BL. Together with the scaling for the BL thickness such that $\lambda_u \sim Re^{-1/2}$, the scaling for the mean dissipation in the particular case of laminar BL[8] is

$$\overline{\epsilon_u} \sim \nu^3 L^{-4} \text{Re}^{5/2}. \quad (6)$$

Combining (3), (5) and (6), one recovers the laminar scaling [12, 3, 16]

$$\text{Re} \sim \text{Ra}^{2/5} \text{Pr}^{-4/5}, \quad (7a)$$

$$\text{Nu} \sim \text{Ra}^{1/5} \text{Pr}^{1/10}. \quad (7b)$$

By analogy to the notation in the GL theory for RBC [4, 16], this scaling regime is denoted as I_l , where the subscript l stands for low-Pr fluids. With decreasing Pr and/or increasing Ra, the bulk dynamics is driven by the large-scale overturning flow whose horizontal length scale is L . In this case, it is the large-scale velocity U which drives the dissipation of kinetic energy and the latter is given by

$$\overline{\epsilon_u} \sim \nu^3 L^{-4} \text{Re}^3. \quad (8)$$

From (3), (5) and (8), it follows that low-Pr HC exhibits dependences of the form

$$\text{Re} \sim \text{Ra}^{1/3} \text{Pr}^{-2/3}, \quad (9a)$$

$$\text{Nu} \sim \text{Ra}^{1/6} \text{Pr}^{1/6}, \quad (9b)$$

where this scaling regime is denoted as II_l [see Fig. 2(b) and ref.[16]]. Note that these scalings are only observed for $\text{Pr} \lesssim 10^{-2}$ where the large-scale flow spans the full depth of the domain [see Fig. 1(a)]. For intermediate Pr, the size of the turbulent overturning flow decreases with increasing Pr, from a deep to a shallow region [see Fig. 1(a-b)]. Similarly, the dissipation increases linearly with increasing Pr and eq. (3) together with eq. (8) can be modified to account for that transitional regime such that

$$\overline{\epsilon_u} \sim \nu^3 L^{-4} \text{Re}^3 \text{Pr}, \quad (10a)$$

$$\text{Nu} \sim \text{Re}^{1/2} \text{Pr} \quad (10b)$$

which is verified empirically in our DNS [see Fig. 3(e) and Fig. 4(b)]. Combining eq. (5), and eq. (10a-b)) provides a correction for this Pr transition in the II_l regime

$$\text{Re} \sim \text{Ra}^{1/3} \text{Pr}^{-1}, \quad (11a)$$

$$\text{Nu} \sim \text{Ra}^{1/6} \text{Pr}^{1/2}, \quad (11b)$$

found in the range $10^{-2} \lesssim \text{Pr} \lesssim 0.2$ [see Fig. 3(b,d)]. Further increasing Pr and for low Ra, the BL thickness λ_u saturates and we observe the laminar scaling reported by Shishkina & Wagner [17]

$$\text{Re} \sim \text{Ra}^{1/2} \text{Pr}^{-1}, \quad (12a)$$

$$\text{Nu} \sim \text{Ra}^{1/4} \text{Pr}^0, \quad (12b)$$

denoted as I_l^* [see Fig. 2(b)]. Increasing Ra and at high Pr, the dynamics are driven by the plume, detached from the bottom [see Fig. 1(b)]. This particular case was theorized by Hughes *et al.*[6] with

a plume model inside a filling box. Here we recast their model according to the SGL theory (i.e. see the plume model definition eq. (2.15)-(2.20) in ref.[6]) and the dissipation in the boundary layer writes

$$\overline{\epsilon_{u,Pl}} \sim \nu^3 L^{-4} \text{Re}^{5/2} \text{Pr}^{-1/2}, \quad (13)$$

where the dissipation now scales with the thickness of the thermal layer, not the kinetic BL and is given by $\overline{\epsilon_{u,Pl}} \sim \nu U^2 / (\lambda_b L)$. Combining (3), (5) and (13)

$$\text{Re} \sim \text{Ra}^{2/5} \text{Pr}^{-3/5}, \quad (14a)$$

$$\text{Nu} \sim \text{Ra}^{1/5} \text{Pr}^{1/5}, \quad (14b)$$

which is denoted as II_u [see Fig. 2(b)].

The slope of the transition regions in the (Ra, Pr) plane, between the laminar regimes I_l , II_l , II_u and I_l^∞ , is determined by matching the Reynolds numbers in these neighboring regimes [4, 16]. Thus, from eqs. (7) and (12), we obtain the slope of the transition region between the regimes I_l and II_l , which is $\text{Pr} \sim \text{Ra}^{1/2}$ and $\text{Pr} \sim \text{Ra}^{-1}$ between II_l and II_u [17]. Each transition region is highlighted by a yellow line in the (Ra, Pr) plane [see Fig. 2(b)] and is estimated from the DNS data, by considering the changes in the $\text{Nu}(\text{Ra}, \text{Pr})$ and $\text{Re}(\text{Ra}, \text{Pr})$ dependencies. Note that the transition is not smooth and suggests that a bifurcation takes place when transitioning from the I_l to II_u regime, and can be affected by the geometry of particular HC setups (as previously suggested in ref.[17]).

In conclusion, we report evidences of a new regime in turbulent simulation of horizontal convection based on scaling arguments at low Pr. The transition occurs from $\text{Re} \sim \text{Ra}^{2/5} \text{Pr}^{-4/5}$, $\text{Nu} \sim \text{Ra}^{1/5} \text{Pr}^{1/10}$ to $\text{Nu} \sim \text{Ra}^{1/6} \text{Pr}^{1/6}$, $\text{Re} \sim \text{Ra}^{1/3} \text{Pr}^{-2/3}$ at low Pr and sufficiently large Ra and then $\text{Re} \sim \text{Ra}^{2/5} \text{Pr}^{-3/5}$, $\text{Nu} \sim \text{Ra}^{1/5} \text{Pr}^{1/5}$. Our results, integrate previous evidence from Shishkina & Wagner [17] and the model of Hughes *et al.* (see ref. [6]) in the SGL theory of HC (see ref. [4, 16]). The transition to the turbulent limiting regime denoted as IV_u or the ultimate regime IV_l have yet to be observed (see ref. [16]). It is therefore of particular interest to attain Rayleigh number of $\text{Ra} \approx 10^{15}$ to determine whether core driven turbulent HC regimes can be reached, as suggested in ref.[16].

The authors acknowledge the support of the National Science Foundation Grant Number OCE-1155558 and OCE-1736989.

References

- [1] T. Alboussiere, R. Deguen, and M. Melzani. Melting-induced stratification above the earth's inner core due to convective translation. *Nature*, 466:744–747, 2010.
- [2] J. Bloxham and A. Jackson. Fluid flow near the surface of earth's outer core. *Rev. Geophys.*, 29(1):97–120, 1991.
- [3] B. Gayen, R. W. Griffiths, and G. O. Hughes. Stability transitions and turbulence in horizontal convection. *J. Fluid Mech.*, 751:698–724, 7 2014.
- [4] S. Grossmann and D. Lohse. Scaling in thermal convection: a unifying theory. *J. Fluid Mech.*, 407:27–56, 2000.
- [5] G. O. Hughes and R. W. Griffiths. Horizontal convection. *Annu. Rev. Fluid Mech.*, 40:185–208, 2008.

- [6] G. O. Hughes, R. W. Griffiths, J. C. Mullarney, and W. H. Peterson. A theoretical model for horizontal convection at high rayleigh number. *J. Fluid Mech.*, 581:251–276, 2007.
- [7] L. Knopoff. Horizontal convection in the earth’s mantle: A mechanism for strike-slip faulting. *Science*, 140(3565):383–383, 1963.
- [8] L. D. Landau and E. M. Lifschitz. *Statistische Physik*. Akademie-Verlag, 1987.
- [9] F. Paparella and W. R. Young. Horizontal convection is non-turbulent. *J. Fluid Mech.*, 466:205–214, 2002.
- [10] P.-Y. Passaglia, A. Scotti, and B. L. White. Transition and turbulence in horizontal convection: linear stability analysis. *J. Fluid Mech.*, 821:31–58, 2017.
- [11] P.-E. Roche, B. Castaing, B. Chabaud, and B. Hébral. Prandtl and rayleigh numbers dependences in rayleigh-bénard convection. *Europhys. Lett.*, 58(5):693, 2002.
- [12] H. T. Rossby. On thermal convection driven by non-uniform heating from below: an experimental study. *Deep-Sea Res.*, 12:9–16, 2 1965.
- [13] A. Scotti. A numerical study of the frontal region of gravity currents propagating on a free-slip boundary. *Theo. Comput. Fluid Dyn.*, 22(5):383, 2008.
- [14] A. Scotti and B. L. White. Is Horizontal convection really ”non turbulent”? *Geophys. Res. Lett.*, 38:L21609, 2011.
- [15] G. J. Sheard and M. P. King. Horizontal convection: effect of aspect ratio on rayleigh number scaling and stability. *App. Math Model.*, 35(4):1647–1655, 2011.
- [16] O. Shishkina, S. Grossman, and D. Lohse. Heat and momentum transport scalings in horizontal convection. *Geophys. Res. Lett.*, 43(3):1219–1225, 2016.
- [17] O. Shishkina and S. Wagner. Prandtl-number dependence of heat transport in laminar horizontal convection. *Phys. Rev. Lett.*, 116(2):024302, 2016.
- [18] O. Shishkina, S. Wagner, and S. Horn. Influence of the angle between the wind and the isothermal surfaces on the boundary layer structures in turbulent thermal convection. *Phys. Rev. E*, 89(3):033014, 2014.
- [19] Olga Shishkina, Mohammad S Emran, Siegfried Grossmann, and Detlef Lohse. Scaling relations in large-prandtl-number natural thermal convection. *Physical review fluids*, 2(10):103502, 2017.
- [20] S.-I. Takehiro. Fluid motions induced by horizontally heterogeneous joule heating in the earth’s inner core. *Phys. Earth Planet. Inter.*, 184(3):134–142, 2011.
- [21] M. F. Taylor, K. E. Bauer, and D. M. McEligot. Internal forced convection to low-prandtl-number gas mixtures. *Int. J. Heat Mass Trans.*, 31(1):13 – 25, 1988.

This figure "figure1.png" is available in "png" format from:

<http://arxiv.org/ps/1805.11741v1>

This figure "figure2.png" is available in "png" format from:

<http://arxiv.org/ps/1805.11741v1>